4th IASPEI / IAEE International Symposium:

Effects of Surface Geology on Seismic Motion

August 23–26, 2011 · University of California Santa Barbara

CONSISTENCY OF GROUND MOTION PARAMETERS FROM NON-LINEAR EMBANKMENT ANALYSES

Richard J. Armstrong
Division of Safety of Dams
Dept. of Water Resources
Sacramento, CA 95818
USA

Erik J. Malvick
Division of Safety of Dams
Dept. of Water Resources
Sacramento, CA 95818
USA

Jeffrey K. Howard
Division of Safety of Dams
Dept. of Water Resources
Sacramento, CA 95818
USA

ABSTRACT

Spectral acceleration and Arias Intensity are used by the California Division of Safety of Dams as target parameters for developing ground motions. The goal of the research presented is to understand the consistency of computed embankment deformations for a relatively large set of design ground motions that meet both S_a and I_a targets under different foundation conditions using non-linear deformation analyses. For this study, forty motions representing M7 and M8 seismic events in California (twenty motions each) were input as dynamic loads into a numerical model of an embankment dam. The model is representative of a typical modern well-compacted zoned embankment dam that consists of a clayey central core with coarse-grained shells. The embankment was analyzed for two foundation conditions: (1) founded on rock and (2) founded on medium-dense alluvium that is susceptible to liquefaction. The non-linear deformation analyses were conducted using the finite-difference program FLAC. The variation of embankment deformation and ground motion parameters for the two sets of ground motions and two foundation conditions is presented and discussed.

INTRODUCTION

The California Division of Safety of Dams (DSOD) manages an inventory of over 1,200 dams. Given the dam safety implications, it is necessary for the seismic analyses of embankment dams to be thorough yet efficient. One method of fulfilling these goals is to utilize a limited number of time histories that are representative of what might be used in a broader analysis, without compromising dam safety requirements.

In practice, it is typical to develop ground motions by matching seed records to site-specific spectral targets as predicted by the NGA relations. However, spectral parameters alone, which only address peak response, are an insufficient basis for developing representative motions for desired design loads, especially for embankment dynamic analyses. As a result, DSOD has added Arias Intensity, I_a, as a target parameter for developing ground motions. Arias Intensity is an example of a ground motion parameter that captures the energy content of motion and is shown to correlate with embankment performance (e.g., Saygili and Rathje 2008).

The goal of this research is to better understand the consistency of computed embankment deformation for a relatively large set of design ground motions that meet both S_a and I_a targets with different foundation conditions using non-linear deformation analyses. For this study, forty ground motions representing M7 and M8 seismic events in California (twenty motions each) were input as dynamic loads into a numerical model of an embankment dam. The embankment model consisted of a typical modern well-compacted zoned dam constructed of a clayey central core with coarse-grained shells. Two foundation conditions underlying the embankment are analyzed. The first condition consists of the embankment directly founded on rock. The second condition consists of the embankment founded on a medium-dense alluvial soil that is susceptible to liquefaction. The non-linear deformation analyses were conducted using the finite-difference program FLAC (Itasca 2009).

This paper begins with a description of the embankment dam and the foundation conditions. Next, the development of the suite of ground motions is described. Details pertaining to the development of the numerical model are then explained. Finally, the numerical results are presented and discussed, and a summary of the findings is provided.

EMBANKMENT DAM AND FOUNDATION CONDITIONS

In this numerical study, a modern well-compacted zoned embankment dam was modeled on a rock foundation (Fig. 1a) and on a 4-m thick alluvial deposit of well-graded medium-dense sand with gravel underlain by the same rock foundation (Fig. 1b). The configuration of the dam and the embankment soils used meet modern design standards. The zoned embankment dam is 15 m (49 ft) high and has a crest width of 6 m (20 ft) with slopes of 2.5H:1V and 3H:1V on the downstream and upstream slopes, respectively. The freeboard of the dam is 2 m. The core is 6 m wide at the crest and 15 m wide at the base of the embankment. For the embankment placed on alluvium, the core extends as a cutoff at a 1H:1V slope through the alluvium to the bedrock. The shell material is assumed to be from the same source as the alluvium (SW with gravel). The core material is low plasticity clay (CL).

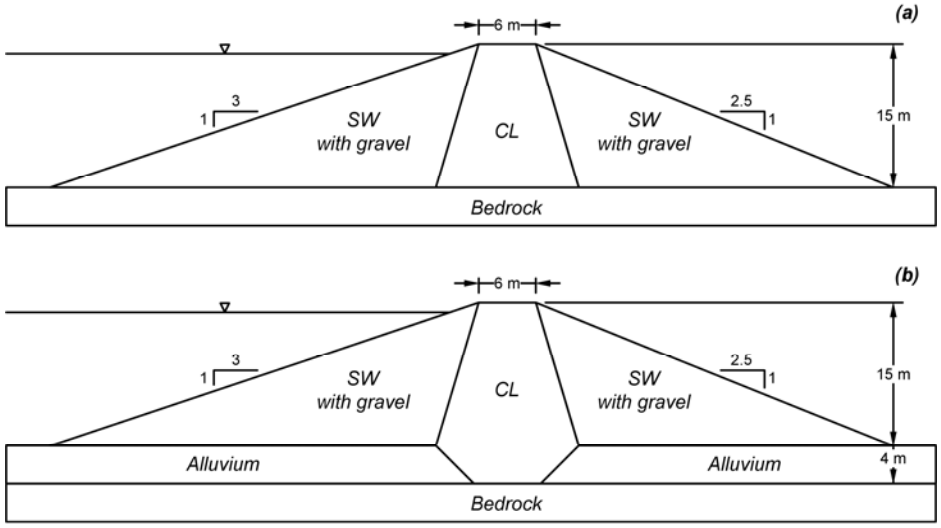

Fig. 1. Zoned embankment dam with the two foundation configurations considered in the study; (a) bedrock, and (b) alluvium underlain by bedrock.

Material properties for the model are chosen to represent typical properties of a modern well-compacted zoned embankment, stiff rock, and medium-dense alluvium. The selected properties for this study are presented in Table 1. A representative $(N_1)_{60}$ was assigned to the cohesion-less materials (e.g., shell and alluvium), and the remaining properties were estimated from these values. Note that for the cohesion-less materials, the relative densities (D_r) of the compacted shell and medium-dense alluvium are approximately 93% and 66%, respectively. For the core material, typical values were chosen based on experience from previous dam construction and from literature. The rock foundation was assigned a shear wave velocity (V_s) of 1000 m/s, representing stiff rock.

Table 1. Material properties of dam and foundation

Zone	*Density*	*Seepage*		*Elasticity*		*Strength*				
	γ_{total} (kN/m^3)	n	k (m/s)	V_{s1} (m/s)	υ	$(N_1)_{60}$	ϕ' (deg)	c' (kPa)	ϕ (deg)	c (kPa)
Shell	20.5	0.34	$1{\cdot}10^{-2}$	217	0.30	40	49.5[a]	–	–[b]	–
Core	21.5	0.28	$1{\cdot}10^{-6}$	206	0.30	–	24	21.6	18.0	16.8
Alluvium	19.9	0.38	$2{\cdot}10^{-2}$	185	0.30	20	36.0	–	–[b]	–
Bedrock	24.0	0.40	$1{\cdot}10^{-10}$	1000	0.30	–	–	–	–	–

Notes: [a] Friction angle at 1 atm. Change in friction angle follows the following relationship: $\phi' = 49.5\text{-}6.6log(\sigma'_h/P_a)$.
[b] Total (undrained) friction angle not a required input into the material constitutive model used.

DEVELOPMENT OF SUITE OF GROUND MOTIONS

Overview

Two sets of twenty input motions for M7 and M8 scenarios were developed for a rock condition (V_{s30} = 1000 m/s). Target spectra were developed using the geometric mean of NGA attenuation formulas. The Idriss (2008) formula was excluded because the ground motions used in this study were the same as those used by Malvick et al. (2011) where S_a estimates were made based on V_{s30} values that Idriss (2008) does not address. Arias Intensity (I_a) targets were developed using 84th percentile results from Travasarou et al. (2003) and Watson-Lamprey et al. (2006); the latter was evaluated using guidance from Watson-Lamprey (2009). Seed records with conditions similar to those being modeled were spectrally matched and carefully scaled to within 5% of the target S_a and 10% of the target I_a. A looser I_a fit is consistent with the greater variance of I_a predictions. Spectral matching was performed using the RSPMatch module in EZFRISK (Risk Engineering 2009), and the target I_a was achieved by adjusting initial scale factor, which determines the number of wavelets that participate in reaching target response spectral amplitudes. Spectral matching output was also screened based on whether the non-stationary (time-varying) characteristics of the original seed motions were preserved. The final motions were base-line corrected and rechecked for spectral target fit.

M7 Scenario

The target parameters for the M7 input motions (V_{s30} = 1000 m/s) were developed for a strike-slip, near-source condition with distance R_{rup} = 5 km. Directivity was not included, to avoid complications in the interpretation of results. The M7 84th percentile input motion targets are *PGA* = 0.56g and I_a = 3 m/s.

The twenty motions representing this scenario were developed using seed records chosen from the PEER database (e.g., Chiou et al. 2008) to best represent the scenario conditions stated. Due to database limitations, the seed record criteria were relaxed to rupture distances within 20 km, M = 6.8 to 7.15, and V_{s30} > 450 m/s. Dam abutment records, records requiring more than 4x scaling, and adjacent records (i.e., recordings within 500 m) were initially eliminated. To obtain the targeted twenty motion records, however, two records with nearby counterparts and one record requiring 6x scaling was used. Table 2 and Fig. 2 show the target parameters: peak ground acceleration (*PGA*) and Arias Intensity (I_a). A statistical summary of the motions including the coefficient of variation, *COV*, is shown in Table 2.

M8 Scenario

The target parameters for the M8 scenario were determined like the M7 event: with R_{rup} < 1 km and no directivity. The resulting 84th percentile targets for the V_{s30} = 1000 m/s condition are *PGA* = 0.87 g and I_a = 9.5 m/s.

Only one near-source M8 strong motion record was available (2002 M7.9 Denali earthquake station PS-10), so to gather twenty M8 input rock motions, seed records from numerical simulations were required. These seed motions were taken from a set of 30 single-component simulations representing a "rock" site condition 7.5 km from a M8 event, which were developed by Walt Silva using stochastic finite-fault modeling and randomized slip. This set was one of several simulated motion sets provided to NGA modelers (Wong, 2004). One characteristic of these motions is that they lack long period content relative to NGA expectations for 4 < *T* < 10 sec, thus spectral matching beyond a 4-second response period could add unnatural long-period wavelets with significant peak velocities (e.g., > 50 cm/s). For this analysis, long period motion is not critical, so spectral matching was limited to *T* < 5 sec. Table 2 and Fig. 2 summarize the final suite of motions developed.

Table 2. Statistical summary of "outcrop" motion properties used as base (input) motions for modeling

	M7					M8				
	Target	Mean	Median	Std. Dev.	COV	Target	Mean	Median	Std. Dev.	COV
PGA (g)	0.56	0.55	0.55	0.02	0.04	0.87	0.88	0.89	0.04	0.05
I_a (m/s)	3.0	3.04	3.03	0.08	0.03	9.5	9.73	9.77	0.48	0.05

It is notable that the *COV* for both *PGA* and I_a are similar, showing that the looser fit to I_a targets is justified, and the suite of motions is consistent for each event. This consistency will provide a good basis for evaluating the ground motion parameters when propagated through the embankment models.

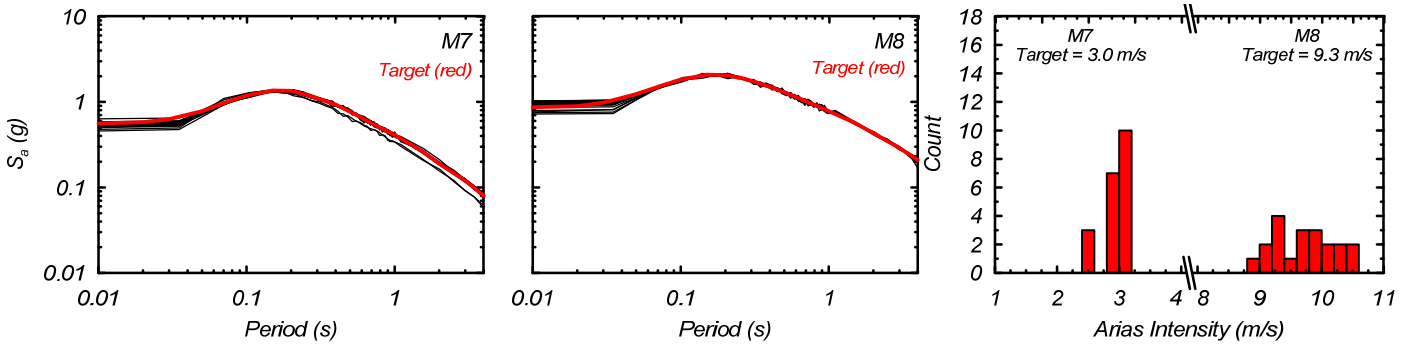

Fig. 2. Spectral accelerations and Arias Intensity distribution for "outcrop" (V_{s30} = 1000 m/s) ground motions for M7 and M8 events.

NUMERICAL MODEL DEVELOPMENT

Overview

The non-linear deformation analyses (NDA) were conducted using the commercial computer program FLAC (Itasca 2009). This finite difference program uses an explicit solution scheme and is well-suited for performing deformation analyses with non-linear material response and large geometry changes associated with instability. The explicit solution satisfies the equations of motion at each nodal mass for every time step. The primary drawback is that FLAC requires very small time steps to avoid numerical instability.

Mesh generation

The meshes used for simulating the embankment underlain by the two foundation configurations (alluvium or rock) are shown in Fig. 3. Each mesh was discretized so that the largest zone (i.e., element) size in the embankment model was around 1 m, sufficient to transmit motions with wavelengths larger than approximately 10 m.

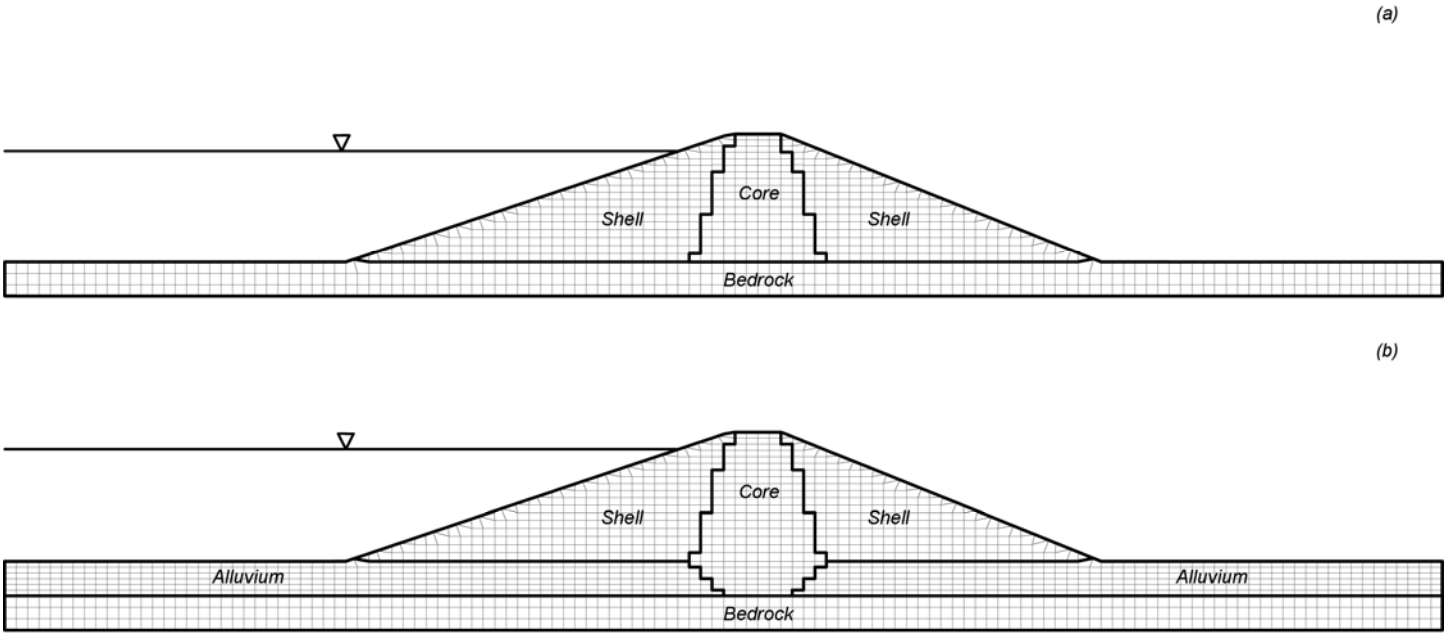

Fig. 3. Finite difference mesh used to simulate embankment underlain by the two foundation configurations; (a) rock and (b) alluvium.

Material constitutive model selection and calibration

The constitutive models were chosen to capture key behavior of the embankment zones and foundation. The bedrock was assumed to be stiff and non-deformable and was modeled using an elastic constitutive model. During the static analysis, the alluvium and embankment zones were modeled with the Mohr-Coulomb constitutive model. The Mohr-Coulomb model is elastic-perfectly-plastic with yielding defined by the material cohesion and friction angle.

During the dynamic analysis, the alluvium and shell were modeled with the UBCSAND constitutive model (Byrne et al. 2004) because these materials are expected to generate pore-water pressures, which are not modeled well with the Mohr-Coulomb model. The UBCSAND model is described as an incremental effective stress model where plastic shear strains accumulate with increases in stress ratio (τ/σ'). Given an increment of plastic shear strain and a constant volume friction angle (ϕ'_{cv}), plastic volumetric strains are contractive for (τ/σ') < sin ϕ'_{cv} and dilative for (τ/σ') > sin ϕ'_{cv}. Hence, in undrained shear loading, the model can capture the increase and decrease of effective stress due to volumetric strains resulting from material contractive or dilative behavior. To avoid unnecessary deformation in the alluvium at the boundary of the model, two columns of zones were not converted to UBCSAND but remained as Mohr-Coulomb with drained strengths.

The input parameters required in the UBCSAND model were chosen based primarily on the calibration performed by Beaty and Byrne (2011). Beaty and Byrne calibrated specific input parameters to the $(N_1)_{60}$ of the soil based on the expected cyclic undrained behavior of sand (e.g., liquefaction triggering and the effects of confinement and static shear stress).

The phreatic surface was developed based on a seepage analysis using the permeability of the materials in Table 1. The embankment material in the core was assumed to behave drained above the phreatic surface and undrained below the phreatic surface. The Mohr-Coulomb model was used for both conditions with an effective strength envelope defined for the soil above the phreatic surface and a total strength envelope defined below the phreatic surface. Stiffness degradation during shearing and the hysteretic damping were captured with the hysteretic damping model available in FLAC. The target G/G_{max} and damping curves for the core were based on Vucetic and Dobry (1991) for a PI = 15.

Static and dynamic analyses

The embankment and alluvium were constructed in layers. To ensure a realistic static horizontal earth pressure condition (K_0) prior to shaking, the K_0 was checked at three different stages during the construction of the numerical model, and the horizontal stresses were reinitialized if the K_0 was outside the range of 0.4 to 0.8.

During the dynamic analysis, 0.5% of Rayleigh stiffness and mass-proportional damping were assigned to the soil foundation and embankment and 1.0% to the rock, all with the minimum frequency equal to the predominate frequency of the model of 3.5 Hz. The UBCSAND model incorporates hysteretic damping, so the Rayleigh damping is only required for high-frequency motion, for elastic response, and to dissipate numerically generated noise.

The velocity time histories $v(t)$ of ground motions developed for the rock outcrop were converted to a shear stress time history (τ) applied to the base of the model using the relationship $\tau = -\rho V_s v(t)$, where the density (ρ), shear wave velocity (V_s), and velocity time history ($v(t)$) are specified for the row of zones directly above the base of the model. An elastic half-space below the bedrock boundary was created by adding viscous dashpots along the base of the model in the x-direction to damp out downward propagating waves. Free-field conditions at the lateral boundary were enforced using the free-field boundary available in FLAC.

RESULTS

Embankment deformations

Embankment deformations were significantly larger for the embankment placed on soil susceptible to liquefaction than when placed directly on rock for both the M7 and M8 motions. This is shown in Fig. 4 with the distribution of the computed peak embankment crest displacement ($\Delta = \max((\Delta_x^2+\Delta_y^2)^{1/2})$) for the M7 motions (Fig. 4a) and for the M8 motions (Fig. 4(b)) with the tabulated mean, median, standard deviation, and coefficient of variation (COV). The reason for the larger embankment deformations with the soil foundation was the instability caused by large shear strains during liquefaction of the alluvium. Contours of maximum shear strain ($\gamma_{max} = \frac{1}{2}((\varepsilon_x-\varepsilon_y)^2+4\varepsilon_{xy}^2)^{1/2}$) after shaking are shown in Fig. 5 overlying the underformed geometry for both embankments from a specific M7 motion (scaled from the Lamont 531 seed record recorded from the 1999 Ducze, Turkey earthquake). In this figure, high

shear strains are seen in the alluvial layers with upstream and downstream slip surfaces that extend through the core and along the alluvial deposit. In contrast, shear strains are significantly lower for the embankment founded on the rock and are isolated primarily along the surface of the embankment.

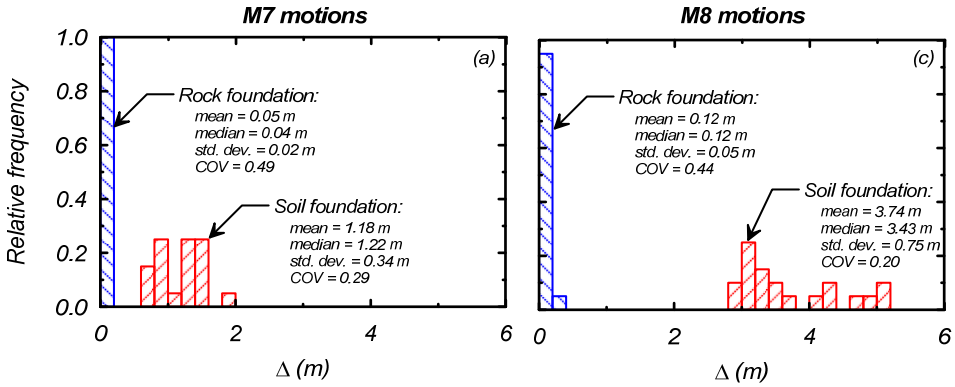

Fig. 4. Distribution of peak embankment crest displacement (Δ) for M7 and M8 events on the rock and soil foundations.

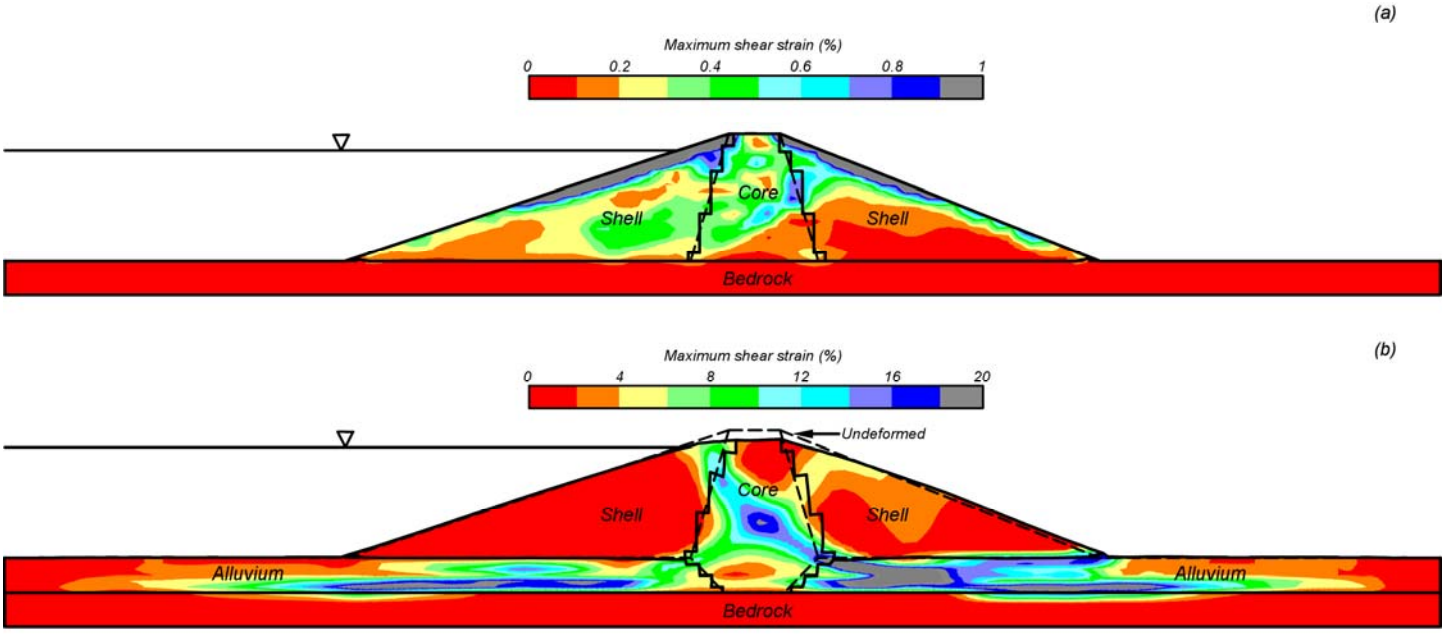

Fig. 5. Deformed grid with contours of maximum shear strain for both foundation conditions. Also included is the shape at the surface of the embankment before shaking. Mesh removed from graph for clarity.

In addition to the increase in mean or median peak crest displacement, the variation of computed peak crest displacement (in terms of standard deviation) increased significantly (Fig. 4). Deformations for the rock foundation model are low for all ground motions, which strongly suggests adequate performance. Conversely, for the twenty M8 motions with the soil foundation, displacements are very large relative to the available freeboard and dam height (i.e., predict overtopping), suggesting inadequate seismic performance. For the twenty M7 motions on the soil foundation, the design conclusions are less clear; a small subset of the ground motions compute crest displacements approaching the available freeboard (note that crest displacement includes both horizontal and vertical components and the computed settlement would be lower), whereas another small subset of ground motions resulted in computed crest displacements that are less than half the available freeboard. If the first subset of motions had been chosen for analyses, the dam would be determined inadequate, while the latter subset may lead to a conclusion that the dam would perform sufficiently.

Spectral accelerations and Arias Intensity

Although the twenty M7 and twenty M8 ground motions input at the base were constrained to S_a and I_a targets, the value of these parameters changed significantly when propagated through the soil or rock foundation and the embankment. This is shown by the distribution of the crest peak horizontal acceleration, *PHA* (Fig. 6a and 6e) and crest Arias Intensity, I_a (i.e., Fig. 6c and 6g), and their distribution when normalized by their median (i.e., Fig. 6b, 6d, 6f, and 6h). The tabulated mean, median, standard deviation, and coefficient of variation (*COV*) are also included for these crest values as well as the mean and median at the input base (the "at depth" or "with-in" motion are related to the developed "outcrop" motion).

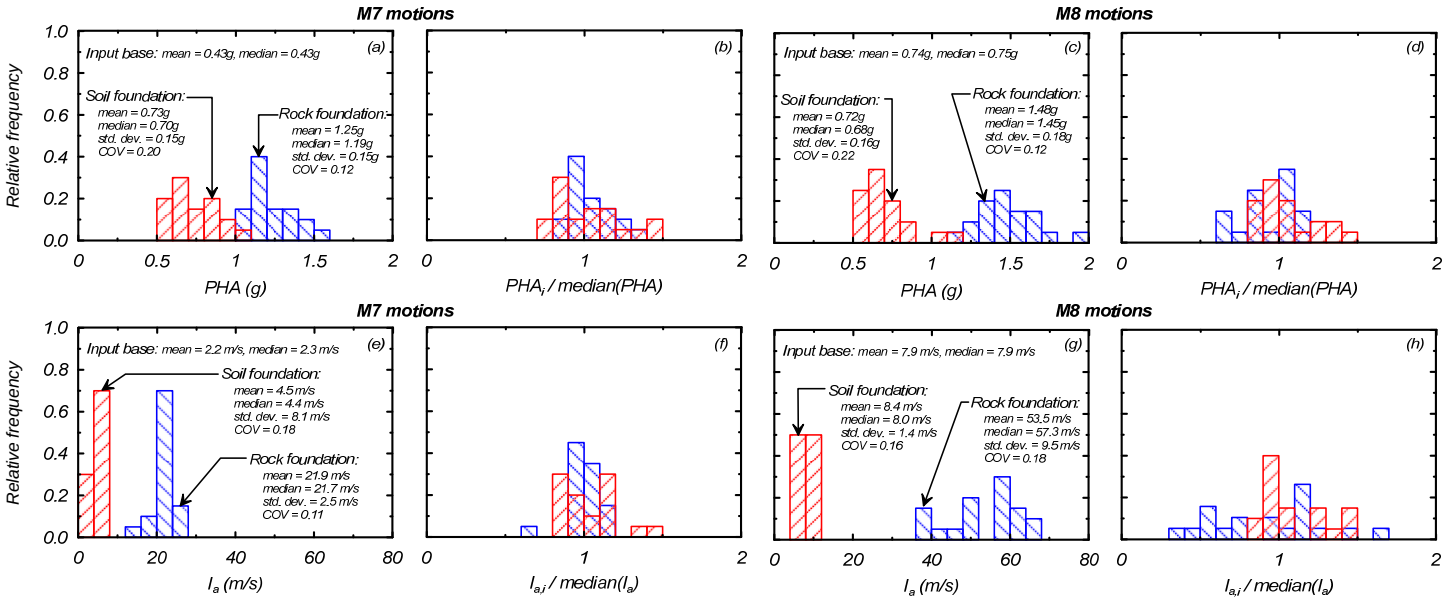

Fig. 6. Distribution of peak horizontal acceleration (*PHA*) and Arias Intensity (I_a) at the crest of the embankment for M7 and M8 events on the rock and soil foundations.

For the M7 motions, the *PHA* and I_a were amplified at the crest relative to the base with the greatest amplification for the rock foundation. Similarly, the *PHA* and I_a for the M8 motions were amplified at the crest relative to the base for the rock foundation but were actually deamplified for the soil foundation. The decrease in *PHA* and I_a is due to significant yielding of the alluvial layer as a result of liquefaction. This is seen by plotting the response spectrum for 5% damping (Fig. 7) at the crest of the embankment for both M7 and M8 motions and both foundation conditions (response spectrum at the base is also included). For the M7 motions, the effect of significant yielding of the alluvium (due to liquefaction) damped out energy and decreased the motion passed into the embankment and thus reduced the crest S_a (or PHA) and the crest I_a. However, there was no significant attenuation in the motion. For the M8 motions, there was both significant damping and attenuation of motion due to considerable liquefaction of the alluvium. The alluvium filtered out the high-frequency motion, whereas the embankment on the rock foundation amplified these higher frequencies. This can be most clearly seen by comparing the S_a at a period of 0.3 seconds.

Given the different scales of the *PHA* and I_a, each value was normalized in Fig. 6 by its median to compare the variation in the crest value (similar comparison could be made by comparing the COV). For the M7 motions, the variation in *PHA* and I_a are similar, although the standard deviation is much larger due to the different scales of *PHA* an I_a. For the M8 motions the crest *PHA* and I_a for the soil foundations were similar, whereas the I_a for the rock foundation condition showed more variation than the *PHA*.

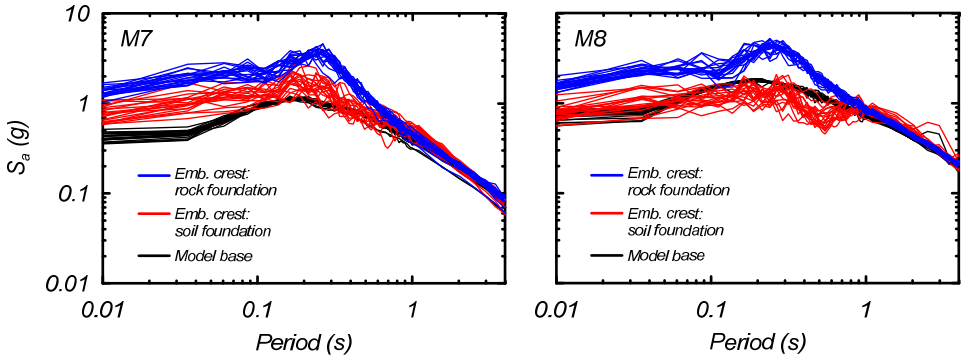

Fig. 7. S_a computed at the embankment crest and model base for both foundations.

SUMMARY

A suite of twenty M7 and twenty M8 ground motions were developed that met both S_a and I_a targets. These forty ground motions were input into a non-linear finite-difference analysis of a 15 m high well-compacted zoned embankment underlain by either a rock foundation or an alluvium foundation. The soil foundation modeled was medium-dense sand that developed excess pore-water pressures during strong dynamic loading.

It was found that for each set of M7 or M8 motions, deformations increased for the embankment founded on the soil foundation due to instability of the embankment caused by liquefaction of the alluvial layer. Additionally, the variation in embankment displacement was greater for the soil foundation than rock condition and the M8 than M7 motions.

The response spectrum and Arias Intensity at the crest of the dam differed depending on the foundation condition modeled. For the rock foundation, both response spectrum and Arias Intensity were amplified. For the soil foundation, the significant yielding of the soil due to liquefaction damped out and attenuated motions, resulting in lower peak horizontal accelerations at the crest with elongation of the period of motion, and subsequently lower I_a at the crest relative to the rock foundation.

This numerical study demonstrates the complexities of performance measures (i.e., crest displacement) for a relatively large set of design ground motions. Further study with additional ground motion sets representing other earthquake scenarios and modeling other embankment configurations would further help to understand the strengths of limitations of the design ground motion parameters. Development of several suites of ground motion with only S_a targets could also be used to help understand the strengths and limitations of I_a as an additional target value for ground motion development.

ACKNOWLEDGEMENTS

Comments from Mr. Wallace Lam from the Division of Safety of Dams led to significant improvements in the manuscript. Although this research was supported by the California Department of Water Resources Division of Safety of Dams, the views expressed are those of the authors and do not necessarily represent the views of the Division.

REFERENCES

Beaty, M. and Byrne, P. [2011]. “UBCSAND Constitutive Model”. Documentation Report: UBCSAND Constitutive Model on Itasca Web Site.

Byrne, P., Park, S., Beaty, M., Sharp, M., Gonzalez, L., and Abdoun, T. [2004]. “Numerical Modeling of Liquefaction and Comparison with Centrifuge Tests”. Canadian Geotechnical J., Vol. 41, No. 2, pp. 193-211.

Chiou, B., R. Darragh, N. Gregor, & W. Silva [2008], “NGA Project Strong-Motion Database”, Earthquake Spectra, Vol. 24, No. 1, pp. 23-44.

Idriss, I. M. [2008], “An NGA Empirical Model for Estimating the Horizontal Spectral Values Generated by Shallow Crustal Earthquakes”, Earthquake Spectra, Vol. 24, No. 1, pp. 217-242.

Itasca. [2009]. "*FLAC, Fast Lagrangian Analysis of Continua, User's Guide*", Version 6.0, Itasca Consulting Group, Inc., Minneapolis, Minnesota.

Malvick, E., Armstrong, R., and Howard, J. [2011], "Consistency of Ground motion Parameters from Site Response Analyses with Empirical Predictions", 4th IASPEI/IAEE International Symposium: Effects of Surface Geology on Seismic Motion, Santa Barbara, California, August 23-26, 2011.

Risk Engineering, Inc. [2009], "*EZ-Frisk Software for Earthquake Ground Motion Estimation*", Ver. 7.60, Computer Software.

Saygili, G. and E. M. Rathje, E. M. [2008], "Empirical predictive models for earthquake-induced sliding displacements of slopes", Jour. Geotech. Geoenv. Engrg., Vol. 134, No. 6, pp. 790-803.

Travasarou, T., J. D. Bray, and N. A. Abrahamson [2003]. "Empirical Attenuation Relationship for Arias Intensity", Earthquake Engineering and Structural Dynamics. Vol. 32, pp. 1133-1155.

Watson-Lamprey, J., and N. Abrahamson [2006], "Selection of Ground Motion Time Series and Limits on Scaling", Soil Dynamics and Earthquake Engineering, Vol. 26, pp. 477-482.

Watson-Lamprey, J. [2009], Disc. on Input Params. for Arias Intensity Predictions, Personal communication with J. K. Howard.

Wong, I. [2004], "Synthetic Time Histories for the Second Tehachapi Afterbay Embankment", URS Corporation report for DWR-DOE, dated January 9, 2004.

Vucetic, M. and Dobry, R. [1991], "Effect of Soil Plasticity on Cyclic Response" Jor. Geotechn. Geoenv. Engrg. Vol. 117, No. 1, pp. 89-107.